

Influence of Structural Properties on Non-Impact Printability of Nanostructured Silica–Polymer Coatings

Jean-Philippe Boisvert* and Aurélien Guyard

CRPP, Université du Québec à Trois-Rivières, Québec, Canada

Jacques Persello

LCMI, Université de Franche-Comté, Besançon, France

The ink jet printing properties of papers coated with two different types of aggregated silica were compared. The structure of the nanoporous aggregates has been investigated with different techniques such as BET and CTAB surface area, Hg porometry and light scattering. The aggregates were thereafter mixed with polyvinylalcohol (PVA). The affinity of the PVA for the silica surface has been studied through adsorption isotherms at pH 5 and 9. It appears that the affinity is much more important at pH 5. PVA–silica slurries were prepared at pH 5 and coated on a non-coated common copier paper and finally printed. Swelling experiments and transmission electron microscopy have been performed on the coatings in order to have additional information on its structure. Black and white image analysis of typographic characters printed on the coatings show that smoothness of contours, gray level, contrast, definition, surface area of the typographic characters depend mostly on the structural properties of the silica, but also on its compatibility with the binder. The combination of both effects determines how important the remaining free porous volume accessible to ink fluids will be, and ultimately how the printing properties, such as shade and pixel resolution, will be. When pores are too large, they become filled with polymer and the silica aggregates lose their absorbency capacity.

Journal of Imaging Science and Technology 47: 256–262 (2003)

Introduction

The development of new digital multimedia devices (scanners, photo and video cameras, etc.), now affordable for all and already installed on computers found in many homes and businesses, puts the paper manufacturers under pressure. The papers used in most of these situations are printed on color ink jet printers. The highly specialized papers used for this purpose must be designed in order to avoid longitudinal and lateral diffusion of colored pigments and promote rapid segregation of ink fluids and the colored pigments. The objective is to keep the colored pigments located where the ink droplet touch the surface first and evacuate the ink vehicle as fast as possible through capillarity induced diffusion in order to leave the dry pigments on the top of the paper sheet. These requirements are now much more acute since new generation of ink jet printers can print both sides of a sheet. Some waiting time is then needed before the other side can be printed, which slows down the printing job.

In general, two types of ink jet papers are found: the polymer rich and the mineral rich papers.¹ As described in Ref. (1), the former type adsorbs the ink solvent by swelling² and filters the colored pigments onto the top of the paper surface, keeping them at the contact area where the droplet touched the surface first. On the other hand, the mineral rich papers use the porous structure of coatings to drain the solvent by capillary effects, still keeping the pigments on top. Two types of porosities may possibly be involved in this draining process: 1) the interporosity, i.e., the porosity created by the more or less dense stacking of mineral particles, and 2) the intraporosity, i.e., the porosity created within porous mineral particles. When conventional coating pigments, e.g., calcium carbonate and clays are used, only interporosity can be created because these minerals are non-porous by nature. The size distribution of coating pigments, the binder (latex) content and type of binder are known to influence the ink transfer process and printability properties, mainly by modifying the pore volume accessible to ink fluids.^{3–8} In the last decade, new porous aggregates with high intraporosity volumes, like amorphous silica aggregates have been specialized and used to enhance the draining capability of the mineral coating, combining both the inter and intraporosity.^{9,10} As reported elsewhere, the porous structure of these later coatings has dramatic effects on the diffusion of ink fluids.⁹

Most of the time, polyvinylalcohol (PVA) is used as binder with silica aggregates^{1,9} and, on this point, the mixture can be assimilated as a hybrid organic inorganic

Original manuscript received September 23, 2002

(*) To whom correspondence should be addressed. Tel: +(819) 376-5075, Fax: +(819) 376-5148, E-mail: jean-philippe_boisvert@uqtr.ca

©2003, IS&T—The Society for Imaging Science and Technology

composite coated on a sheet of paper. The structure of such composites has been thoroughly investigated in recent years, and it has been shown that surface properties of the silica aggregates are of prime importance in the resulting structure, to such a point that many coupling agents are specifically designed to modify the surface properties in order to improve the compatibility between the inorganic component and the organic matrix and insure optimum dispersion of the mineral. In the context of composite material, most of the studies found in the literature usually concern its mechanical properties (elongation and stress at break, elastic modulus, etc.) in relation with surface properties of the filler and/or its structural arrangement within the polymer matrix. For instance, it has been shown from swelling experiments that in the case of a weak polymer/SiO₂ interaction, the polymer distribution is perturbed in the vicinity of the silica surface. In this situation, the solvent diffuses to interface and causes the polymer to desorb almost completely from the filler SiO₂ particles, while the surface remains covered when the interaction is strong.¹¹ It is also well known that the increased number of grafted chains of a coupling agent on the silica surface leads to a higher level of overstrain.¹² Finally, the influence of the polymer/silica interaction on the extent of dispersion (or clustering) of the filler and the importance of surface density of silanol surface sites are also well documented in recent literature.^{13–16} The polymer/SiO₂ interaction can account for the self-assembly of silica aggregates observed with silica primary particles in presence not only with hydrogen bond reactive polymer¹⁶ but also with grafted polymer.¹⁷

Although the relation between mechanical properties of composites and structural arrangement of mineral fillers (and by extension, filler surface properties) has been extensively studied in the context of composite reinforcement, fewer studies have investigated the printability or ink-holding capacity of such kind of “composites” in connection with structure and surface properties of porous SiO₂ “fillers”.

The goals of this study are to identify the interrelations existing between the ink jet printing quality, the structure of the paper coating, the structure of the nanoporous silica aggregates and finally the PVA/SiO₂ interaction. Although much work has been done in the past to understand the relations between the printing quality and the coating structure, fewer studies have focused on the importance of the binder/mineral interaction and of the aggregate structure on the first two parameters. Accordingly, the experimental procedure will allow correlations between surface and structure properties of SiO₂ aggregates, film structure and ink absorbency.

Material

General

All experiments were conducted in distilled and deionized water. The chemical reagents were all analytical grade and were used without further purification. The pH of solutions and suspensions were adjusted to pH 5 and 9 with NaOH.

Synthesis and Characterization of Silica

First, primary silica particles were grown from aqueous silicate solutions neutralized by nitric acid. Sodium silicate was produced by dissolving a pyrogenic silica into a concentrated NaOH solution in order to reach a molar ratio $x = \text{SiO}_2/\text{Na}_2\text{O} = 3.40$. The resulting silicate

solution was thereafter diluted to a silica concentration of 0.57 M. The precipitation of silica was initiated by diluting an initial batch of silicate solution with water to a concentration of 0.004 M; this dilution lowered the pH to 9 and initiates the formation of silica nuclei. They were thereafter allowed to grow and ripen, as described elsewhere.^{18,19} In order to remove the salt, which was a by-product of the reaction, the silica sol was circulated in a tangential ultrafiltration module. During this stage the concentration of the sol was maintained constant by addition of deionized water. The pH of the sol was also kept constant at pH 9. A further ultrafiltration stage without replacement of water was used to concentrate the sol up to a given silica volume fraction. Thereafter, the aggregated products were allowed to coalesce under controlled ionic strength and temperature conditions. In order to obtain the products designated in SNP1 and SNP2, (see Table I), the silica volume fractions of the suspension were adjusted to 0.025 and 0.045 and the ionic strengths were 5×10^{-2} M and 3×10^{-1} M, respectively. The characterization methods used to characterize the porous structure of both products are described just below.

The porosity has been measured by mercury porosimetry with a Quantachrome instrument (Autosorb 60 model). The specific surface areas were measured by low temperature N₂ BET adsorption isotherms also with a Quantachrome Autosorb Instrument. The external surface areas were also probed by hexadecyltrimethylammonium Bromide (CTAB) adsorption as described elsewhere.²⁰

The aggregate size distribution was measured by laser diffraction using a Malvern Mastersizer model E instrument. The slurries were diluted in aqueous electrolyte solutions with the corresponding ionic strength, stirred and ultrasonicated *in situ* five minutes before measurements. The particle concentration was imposed by the instrument ensuring optimum operational conditions.

Polymer Characterization

The polyvinylalcohol (PVA) used in this work is a neutral polymer purchased from Fluka (cat. number 9002-89-5). According to the supplier, this polymer has a weight average molecular weight (MW) of 100 Kg/mol and a degree of purity of 99%. In the present study the polymer was used without further purification. Viscosity measurements showed a viscosity-average MW of 107 Kg/mol and a gyration radius (R_g) of 15 nm at pH 5 and 9. The polymer is non-ionized within this pH range. The overlap concentration for this polymer is 8 g/l in water. The mass of the elastic chains was estimated from swelling experiments in water. This yields for the unfilled sample to a number average MW of 7400 ± 400 g/mol. The Flory parameter (χ) in semi-dilute condition was measured by osmometry. The experimental value was 0.499 (at both pH values) which agrees well with $\chi = 0.494$ reported elsewhere.²¹ In dilute concentration, $\chi = 0.47$.²¹

Adsorption Isotherms

SiO₂ suspensions at initial pH 5 or 9 were mixed with increasing concentrations of PVA solutions at same pHs. Five days were allowed for equilibrium at the end of which the suspensions were centrifuged and the total organic carbon (TOC) of the supernatant was measured with a Carbon analyzer (Dohrmann instrument). Only experimental data with (initial TOC-equilibrium TOC)/initial TOC > 0.2 were taken as significant. Calibration

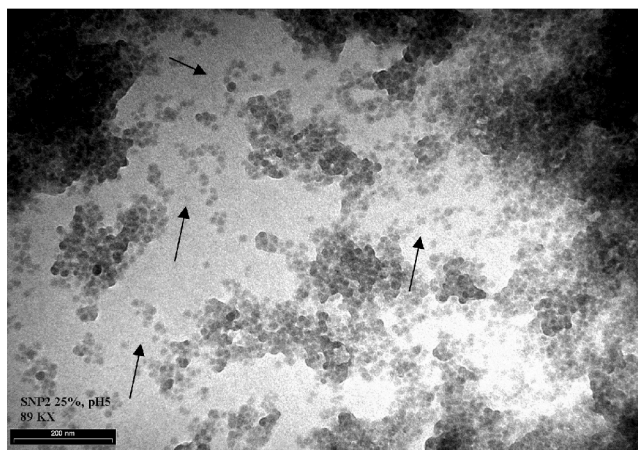
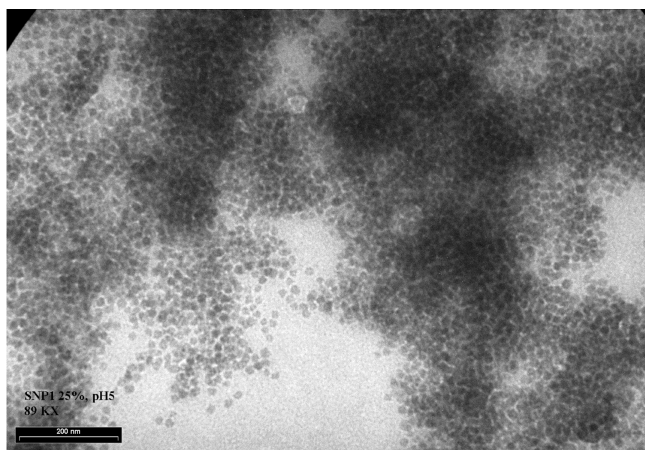


Figure 1. MET micrographs of the SNP1/PVA film (left) and SNP2/PVA film (right). The bar on the micrographs is 200 nm. The silica content is 25% on a dry weight basis.

curve was established with known concentrations of PVA. The standard deviation for 3 consecutive measurements was lower than 5%.

In order to compare the obtained saturation values at full surface coverage with the maximum possible surface coverage on silica, the adsorption isotherms were also performed on nanometric spherical silica particles. The reader is referred elsewhere for full details on the preparation of these particles.^{18,19} The particles are 27 nm in size and the polydispersity index of the suspension is 1.07. In addition to adsorption isotherms, the hydrodynamic thickness δ for saturated layers of PVA on the silica spheres was measured at pH 5 by viscosimetry (results not shown here) and computed through an equation adapted from Einstein's relation.²² The thickness of the adsorbed layer was found to be 10 nm at saturation and pH 5. This value is fairly comparable to what has been reported elsewhere for a very similar system.²² This technique could not be used at pH 9 because the surface coverage was too low to allow reasonable significance in the results.

Film Formation and Coating

The films were prepared in non-adhesive moulds by mixing SiO₂ suspensions ($\phi = 0.02$, pH 5 or 9) with the corresponding PVA solution (5% dwb, pH 5 or 9) in appropriate proportion in order to finish with dry basis volume fractions [SiO₂/(SiO₂+PVA)] ranging from $\phi_{Si} = 0.05$ to 0.35 once the solvent had been evaporated. Prior to evaporation, the PVA surface coverage is well above saturation. At the end of the evaporation process, the films were removed from the moulds and tested for swelling.

The PVA/SiO₂ slurries were also coated on a common non-coated paper (Domtar copier paper), which rates an ISO brightness of 80. The coated device was a lab coater with wired-wound rods (#6 gauge). The sheets were thereafter dried and printed in black and white on a Canon BJC4400 ink jet printer with the ink recommended by the manufacturer.

Electron and Optical Microscopy

Transmission electron microscopy (TEM) sample preparation consisted of immobilizing the PVA/SiO₂ films in a resin and slicing the film with an ultramicrotome. The cross section was fixed onto a coated carbon

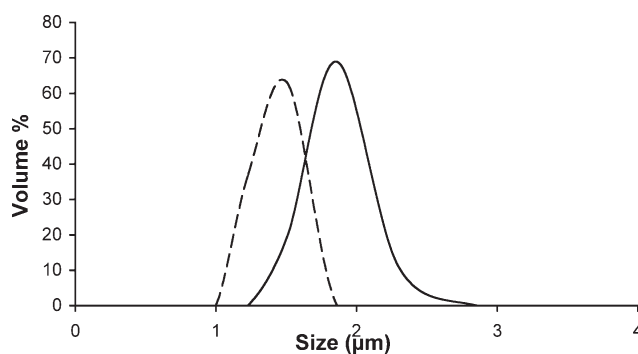


Figure 2. Size distribution of SNP1 and SNP2 aggregates measured by laser diffraction. Dashed line: SNP1, solid line: SNP2.

grid. TEM examination was performed using a Philips instrument operating at 120 kV.

Optical microscopy was used to magnify and image the ink jet printed letters. Images were digitized and processed through an image analysis software (Image SXM, NIH) in order to quantify the gray level and the contour of the printed patterns.

Results and Discussion

The morphological differences between the two products are inferred from the TEM micrographs shown in Fig. 1. Of course, the usual reservations about the interpretation of two-dimensional images resulting from the projection of a three-dimensional object apply here. Moreover, the micrographs show local images of the film structure in which SiO₂ aggregates may have collapsed during the drying process. This hypothesis is strongly supported by laser diffraction measurements showing aggregates with a reasonably clean and narrow monomodal size distribution of 1.5–2 μm large aggregates (see Fig. 2). Such aggregate sizes are not clearly identified in Fig. 1. However, the primary particles inside aggregates are easily identified and appear to be about the same size (13–15 nm) in each of the products. The main differences between the SNP1 and SNP2 structures lies in the way that identical primary objects are assembled into aggregates upon aggregation.

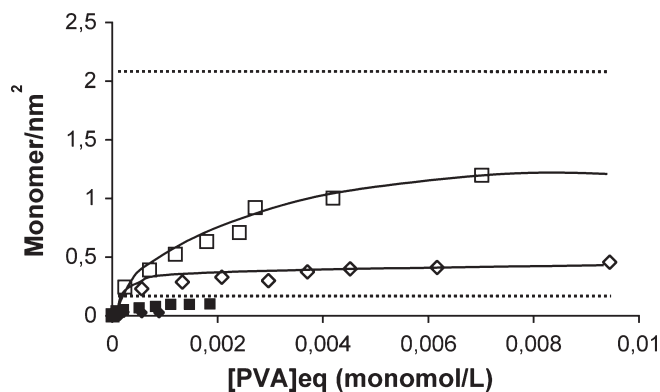


Figure 3. Adsorption isotherms of 100kg/mol PVA on SNP1 and SNP2 at pHs 5 and 9. Squares: SNP2, Diamonds: SNP1. Open symbols: pH 5, Filled symbols: pH 9. The dashed horizontal lines indicate the PVA surface densities at saturation for the silica spheres (reference). The upper line refers to the maximum surface density at pH 5, while the lower line is for pH 9.

This being said, it is clear that the SNP1 and SNP2 aggregates have different structures. Obviously, the SNP1 aggregates are bushier than the SNP2. As indicated by arrows in Fig. 1, some of the objects in the SNP2 product show stick-like structures. Such morphology is nonexistent in the SNP1 product.

The main physical characteristics of the products are grouped together in Table I. Both methods of surface area measurement using different probes (N_2 and CTAB) are concordant, indicating that the entire surface is external. The porous volume measurements support the TEM observation about the different structures of SNP1 and SNP2 products. According to mercury porosimetry measurements reported in Table I, the SNP1 product has smaller pore size and lower porous volume than SNP2. The pore size distribution reveals that 95% of the pores are within 6–10 nm in the SNP1 sample, while they are 15–50 nm in size in the SNP2 sample. This is consistent with the surface area measurements and TEM reported above. The higher connectivity of SNP1 leads to lower surface area, lower pore size, lower porous volume and higher effective density.

Adsorption Isotherms

In order to have a comparative reference regarding the maximum surface coverage to be expected following PVA adsorption, adsorption isotherms were performed on spherical silica particles at pH 5 and 9. Being non porous by nature and perfectly dispersed, one hundred percent of the surface on these particles is available, so the adsorption can take place with no restriction. Thus surface densities at saturation on the spherical particles are considered as reference values to which the saturation limits of the porous aggregates will be compared. The dashed horizontal lines in Fig. 3 indicate these reference values. The upper line refers to the maximum surface density at pH 5, while the lower line is for pH 9. The great difference in the saturation values for the spheres as shown in Fig. 3 can be explained by the surface properties of amorphous silica. Indeed, earlier works on adsorption of neutral polymers on silica have shown that neutral polymers like PEO adsorb on silica through hydrogen bonding with silanol surface sites.^{23,24} A similar behav-

ior is expected with PVA but the better PVA–water interaction makes the surface less “attractive” to PVA. Since the surface density of silanol sites decreases as the pH increases,¹⁸ decreasing surface coverage is expected with PVA as the pH rises from 5 to 9, respectively. At pH 5, surface sites are mostly non-ionized silanol groups (first $pK_1 = 2$) on this material, while at pH 9 more than half are ionized (second $pK_2 = 8$).²⁵

The porosity of the SNP1 and SNP2 products introduce new parameters in the adsorption process. When the polymer adsorbs into pores smaller than the gyration radius of the polymer, two main and opposing effects are involved: the loss of entropy due to the deformation (unfavorable to adsorption) and the gain of enthalpy due to the creation of H-bonds (favorable). Accordingly, lower saturation values are expected with the porous products at a given pH. Here, energy contributions to adsorption related to the H_2O-H_2O , $PVA-H_2O$ and $PVA-PVA$ interactions are neglected since the Flory’s parameter (χ) is very close to 0.5 (theta solvent). Previous polymer characterization has shown that the polymer coil has a radius of gyration of 15 nm and, accordingly, cannot penetrate into pores smaller than about 40 nm without being deformed (coil diameter = $2[R_g(5/3)^{1/2}] = 40$ nm). As reported in Material and Methods, it is recalled that some deformation is expected, even upon unrestricted adsorption. Indeed, the polymer layer thickness is only 10 nm on the curved surface of spherical silica particles.

The energetic arguments developed above regarding the balance between deformation and adsorption could explain the different saturation densities observed with both products at pH 5. As expected, the two porous products have (much) lower saturation densities than the non-porous and dispersed spheres. The difference between the surface densities at saturation is qualitatively consistent with the differences in the product characterization; the surface density at saturation is lower with SNP1 (smaller pore size) than with SNP2 (larger pore size). A higher pore fraction in SNP1 aggregates remains then free of any polymer and might readily adsorb ink (see below). Actually, 80% of the SNP1 surface is not accessible to the polymer compared to 50% with SNP2, taking the saturation limit for spherical silica particles as a reference. Accordingly, higher printing quality is expected with SNP1.

The saturation limit at pH 9 is very low for all products and illustrates how poor is the affinity between PVA and the silica surface at this pH. It is suggested that the gain in enthalpy would be too low (due to the low H-bonding surface site) to counterbalance the loss of entropy due to extensive deformation, as a result that almost no adsorption occurs.

The experimental conditions during the preparation of the slurries, used for coating and preparation of films, were somewhat different to that occurring in adsorption experiments because the polymer concentration was much higher in the slurries. The polymer concentration is well above the overlap concentration and consequently the polymer coils are entangled (semi-dilute regime), as described by deGennes.²⁶ However, the above arguments regarding the energetic cost of polymer deformation and its limiting effect on adsorption remain fully appropriate.

Swelling Behavior

Once dry, the films were re-swollen in water until equilibrium. As can be seen in Fig. 4, the incorporation of silica aggregates into PVA restricts the swelling. Two

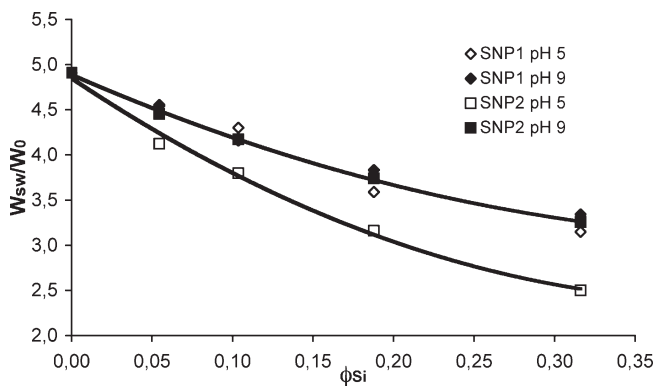


Figure 4. Swelling of SNP1/PVA and SNP2/PVA films at pH 5 and 9. They axis represents the weight fraction of the swollen films compared to that of the dry film against the volume fraction of silica in the dry film $\phi_{Si} = [SiO_2/(SiO_2 + PVA)]$.

effects can possibly explain this behavior: first, the silica on itself does not swell at all, and so the water uptake by the film decreases with the increasing volume fraction of silica. Second, the inclusion of PVA into the pores of aggregates also reduces its extensibility or swelling capacity. But since the re-swelling is the same for SNP1 at both pHs, while the surface coverage are significantly different, the later effect is obviously not the most important. This just reflects the fact that the volume of polymer included in intraporosity of aggregates (intraaggregate inclusion) is relatively unimportant compared to that of bulk polymer (at most 1%, well within the experimental error).

Interestingly, the restricted swelling effect is the same for all samples but the SNP2 product at pH 5. This particular difference between the latter product and the others can be explained by an additional (third) effect which superimposes to the first two: the good affinity of PVA toward the silica surface at pH 5 makes the (accessible) surface much more readily wetted by the polymer matrix. As the mean volume fraction increases, open aggregates form an open network, which progressively spans all over the film. Because of the higher degree of openness of the SNP2 aggregates, larger polymeric domains are possibly trapped inside the rigid silica structure and these interaggregate inclusions would have an extensibility (or swelling) capacity lower than that of the bulk polymer. Such a behavior has been reported elsewhere²⁷ on similar organic-inorganic systems. On the other hand, because of the poor (non-wetting) PVA/SiO₂ interaction at pH 9, the SNP2 aggregates collapse together into compact agglomerates which lead to the same compact agglomerate structure than with SNP1. The effect of pH on the film structure is obvious from TEM for the present samples and also for the spherical silica particles embedded in PVA (results not shown).

Quoting the Kraus theory,²⁸ one could argue that the SNP2 at pH 5 swells less than that at pH 9 because of the better PVA/SiO₂ interaction at pH 5. A recent study on the structure and re-swelling properties of spherical, and nanometric silica particles dispersed in a PVA matrix has shown that the polymer/SiO₂ interaction at pH 5 is actually not strong enough to restrict the swelling,²⁹ and consequently the Kraus theory will be considered as non applicable in the present case, or its effect non significant.

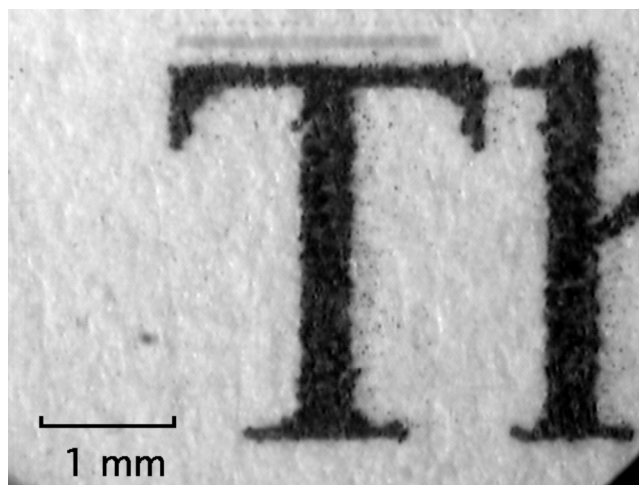


Figure 5. Image of typographic character (capital *T*) ink jet printed on uncoated copier paper (reference). The image was magnified, captured by a digital camera device and processed through an image analysis software. Area: 1.80 mm²; Perimeter: 15.0 mm; gray level: 84 ± 3%. The standard deviation of the gray level represents the deviation from pixel to pixel along the vertical bar of the letter *T*. The standard deviation from letter *T* to letter *T* for gray level is 1%, well within the standard deviation from pixel to pixel.

Structure versus Ink Absorbency

Ink jet printing has been performed on four different types of papers: 1) the uncoated copier paper used as coating support, 2) the copier paper coated with PVA alone, 3) the copier paper coated with the PVA/SNP1 slurry and finally, 4) the copier paper coated with the PVA/SNP2 slurry. In the two latter cases, the SiO₂ volume fraction of the dry coating was 0.35 and pH = 5. The printing quality on the printer was set to intermediate quality for all paper samples, the font type was Times Roman and the font size was 12 point. The corresponding images of the magnified typographic letter *T* were captured with numerical camera devices installed on a stereoscope and processed through image analysis software. The images are presented in Figs. 5–8 and correspond respectively to the four papers described above. No attempts were made either to improve or optimize the results. Actually, the level of development of our systems would rather be classified as preliminary. Accordingly, the differences between the SiO₂ coated and uncoated papers are expected to be enhanced even more as the surface coating conditions and treatment will get improved.

The average gray level, the area and the perimeter of the letter *T* are reported in the figure captions. The gray level is reported in percent where 100% corresponds to black and 0% corresponds to white. The gray level of background is 40% for all pictures. The standard deviation for areas and perimeters is 0.06 mm² and 0.5 mm, respectively. The standard deviation of the gray level from pixel to pixel along the vertical bar of the letter *T* is reported in each Figure. The standard deviation of gray level from letter *T* to letter *T* is 1%, well within the standard deviation from pixel to pixel.

The three coatings are compared to the reference. As can be seen in Figure 6, the PVA coating makes the surface glossier. Ink droplet satellites are observed on the left part of the character presumably because the glossy PVA film makes the ink to rebound in part on

the surface. The smearing of ink is also important. Accordingly, the gray level and perimeter are higher here than with the uncoated reference (see Fig. 5). The PVA coating can be seen as an impermeable coating that prevents the normal ink diffusion but not its lateral smearing. When the SNP1 product is added to the polymer the ink holding capacity of the resulting coating is greatly increased. As can be seen in Fig. 7, the gray level is clearly improved compared to the reference. Some lateral ink diffusion seems to occur since the printed area is somewhat higher, although the perimeter does not significantly differ from the reference. Since the planarity of the surface has suffered from being wetted and dried without particular care during coating, which could have created additional surface roughness, it is not surprising that the definition is not optimum. But obviously, the overall ink holding capacity is very good with SNP1, better than with the other formulations investigated in this study. This is attributed to the high effective void volume, i.e., the volume not occupied by any PVA.

Even though the BET and CTAB surface area is high with SNP2, it is clear from Figure 8 that the printability (gray level, but mostly the lateral diffusion) is bad. This can be explained by the higher pore size, allowing PVA molecules to adsorb on most of the surface area and to occupy most of the voids. In this situation, the porosity is then not effective. On this point, the resulting material can be compared to a PVA film with dense SiO₂ aggregates embedded in the polymer matrix. When the ink hits the surface, the non-porous (impermeable) surface prevents the normal diffusion but not the lateral smearing of ink. Accordingly, the ink holding capacity of SNP2 is poor, similar to that of pure the PVA coating. Again, this effect is surely amplified by the additional roughness caused by the surface preparation.

The intraaggregate structural effects (intraporosity, surface chemistry) are expected to superimpose over the interaggregate structural effects (aggregate distribution, interporosity) and modulate the printing quality. The relative importance of both effects needs to be further investigated.

Conclusion

The printing properties of different paper surfaces have been investigated and correlated to structural parameters and surface properties of the SiO₂ ink holders used in this study. It has been shown that surface area of the two SiO₂ products measured with the N₂ and CTAB probes is not directly correlated with the printing quality. As far as the swelling experiments give indications on the structural arrangement of SiO₂ aggregates within the PVA matrix, the printing quality could depend on this parameter but its relative importance is not clear yet and needs to be studied more deeply. In addition to that, the effective intraporous volume of silica aggregates, i.e., accessible to ink fluids, can explain the printing quality. The effective intraporous volume depends of course, on the porous volume of aggregates prior to the polymer addition but also on the accessibility of this volume. This accessibility depends on the pore size and on the free energy costs of polymer adsorption, which in turn depends on the polymer affinity for the surface (pH). These two effects (distribution of porous aggregates within the matrix and effective porous volume) are pH dependent and determine how the printing properties such as shade and pixel resolution will be. Of course, pores filled with polymer lose their capacity to absorb. ▲

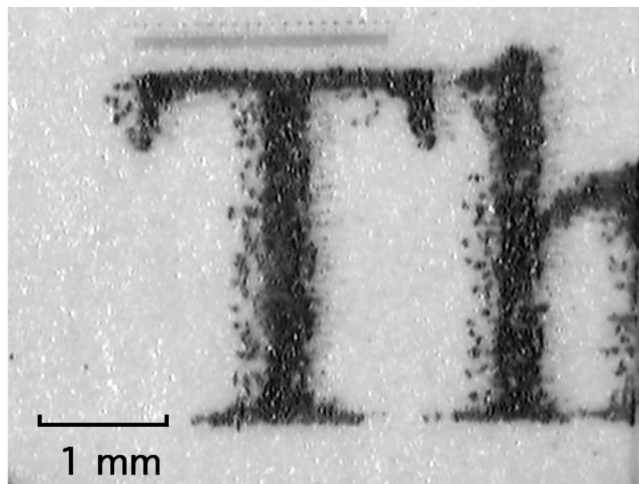


Figure 6. As Fig. 5 but for the pure PVA coated on the reference paper. Area: 1.83 mm²; Perimeter: 19.3 mm; gray level: 81 ± 9%.

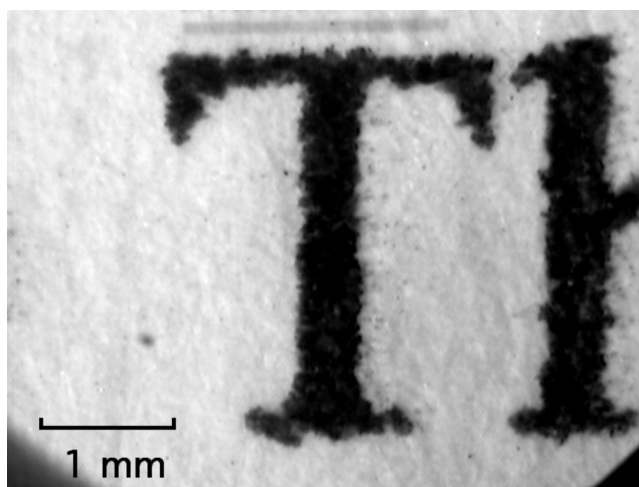


Figure 7. As Fig. 5 but for the SNP1/PVA mixture coated on the reference paper. Area: 2.17 mm²; Perimeter: 15.4 mm; gray level: 90 ± 2%.

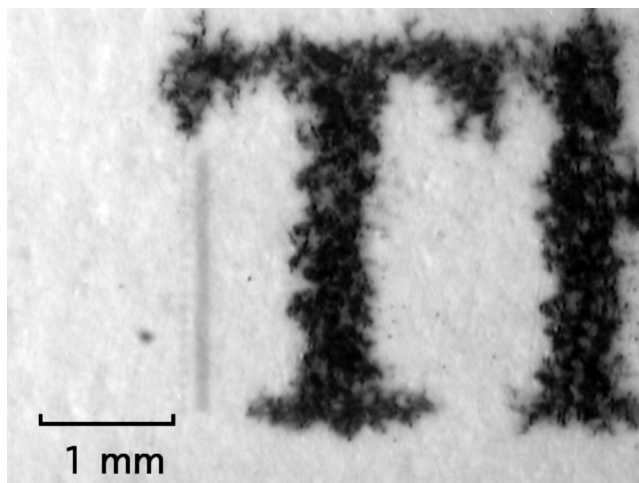


Figure 8. As Fig. 5 but for the SNP2/PVA mixture coated on the reference paper. Area: 2.53 mm²; Perimeter: 23.2 mm; gray level: 81 ± 7%.

TABLE I. Main Characteristics of the Porous Materials Used in This Study.

	BET surface area (m ² /g)	CTAB surface area (m ² /g)	Total porous volume (ml/g)	Mean pore size (nm)	Effective density ^a (g/ml)
SNP1	113	133	0.6	7	0.94
SNP2	196	194	0.9	15	0.73

* The effective density is calculated according to: $1/(1/d_{\text{SiO}_2} + V_p)$ where d_{SiO_2} is the silica density (2.16 g/ml)

Acknowledgment. The authors would like to acknowledge Agnès Lejeune from UQTR for the supply of the TEM micrographs. The Ministère des Relations Internationales du Québec as well as NSERC-International Opportunity Fund are also acknowledged for financial support through research grants.

References

1. D. M. Chapman and D. Michos, *J. Imag. Sci. Technol.* **44**, 418–422 (2000).
2. R. Poeschke and A. Stumpf, *Proc. of IS&T's NIP16 Conf.*, IS&T, Springfield, VA, 1998, p. 266.
3. Y. Xiang and D. W. Bousfield, *J. Pulp Paper Sci.* **26**, 221–227 (2000).
4. G. E. Kowalczyk and R. M. Trksak, *TAPPI J.*, **81**, 181–190 (1998).
5. Y. Arai and K. Nojima, *Proc. TAPPI Coating Conf.*, TAPPI, Atlanta, GA, 1997, pp. 133–142.
6. Y. H. Zang and J. S. Aspler, *J. Pulp and Paper Sci.* **24**, 141–145 (1998).
7. E. Kalela, C. J. Ridgway and P. A. C. Gane, *Proc. Int. Printing Graph. Arts Conf.*, TAPPI, Atlanta, GA, 2002, paper I-3.
8. D. Desjumeaux, D. W. Bousfield, T. P. Glatter, D. W. Donigan, J. N. Ishley, and K. J. Wise, *J. Pulp and Paper Sci.* **24**, 150–155 (1998).
9. D. M. Chapman, *Proc. TAPPI Coating Conf.*, TAPPI, Atlanta, GA, 1997, pp. 73–93.
10. M. Takahashi, T. Sato and M. Ogawa, *Japan TAPPI J.* **42**, 923–931 (1988).
11. A.-M. Hecht, F. Horkay and E. Geissler, *Phys. Rev.* **64**, 041402–1–6 (2001).
12. A. Botti, W. Pyckhout-Hintzen, D. Richter, and E. Straube, *Physica A*, **304**, 230–234 (2002).
13. J. Jianfen and R. Salovey, *J. Mater. Sci.* **34**, 4719–4726 (1999).
14. R. C. R. Nunes, J. L. C. Fonseca and M. R. Pereira, *Polymer Testing* **19**, 93–103 (2000).
15. Q. Deng, J. R. Hahn, J. Stasser, J. D. Preston, and G. T. Burns, *Rubber Chem. Technol.* **73**, 647–665 (2000).
16. J. Jang and H. Park, *J. Appl. Polym. Sci.* **83**, 1817–1823 (2002).
17. C. Becker, B. Kutsch, H. Krug, and H. Kaddami, *J. Sol Gel Sci. Technol.* **13**, 499–502 (1998).
18. R. K. Iler, *The Chemistry of Silica*, Wiley, New York, 1979.
19. J. Persello, A. Magnin, J. Chang, J. M. Piau, and B. Cabane, *J. Rheol.* **38**, 1845–1870 (1994).
20. J. Jansen and G. Kraus, *Rubber Chem. Technol.* **44**, 1287 (1971).
21. K. Lewandowska, D. U. Staszewska and M. Bohdanecky *European Polymer J.*, **37**, 25–32, (2001).
22. F. Lafuma, K. Wong and B. Cabane, *J. Colloid Interface Sci.* **143**, 9–21 (1991).
23. G.P. Van der Beek and M. A. Cohen-Stuart, *J. Phys. (France)* **49**, 1449 (1988).
24. M. A. Cohen-Stuart, G. J. Fleer and J. M. H. M. Scheutjen, *J. Colloid Interface Sci.* **97**, 526 (1989).
25. A. Foissy and J. Persello, *The Surface Properties of Silica*, John Wiley and Sons Ltd., New York, pp. 365–414, 1998.
26. P. G. deGennes, *Scaling Concepts of Polymer Physics*, Cornell University Press, Ithaca, NY, 1979.
27. D. W. McCarthy, J. E. Mark and D. W. Schaeffer, *J. Polymer Sci.* **36**, 1167–1189 (1998).
28. G. Kraus, *J. Applied Polym. Sci.* **7**, 861 (1963).
29. J. Persello, J.-P. Boisvert and A. Guyard, submitted for publication (2002)